Highlight(s)

- 1) Standard covellite phase achieved by simple route.
- 2) Hexagonal structure is attained without use of stabilizing or pH agents.
- 3) Ethanol and Ethylene glycol are used as co-solvent with deionized water (DW).
- 4) This two combinations of co-solvents are examined at 30:70 ml ratio and were not reported before.
- 5) Solvent 1 DW: Ethanol, solvent 2 DW: Ethylene glycol.

Physicochemical and optical properties of Covellite (CuS): A comparative study of two co-solvent assisted synthesis method

Solairajan Shanthosh Shree¹ and SethuramachandraanThanikaikarasan¹*

¹Department of Science and Humanities, Saveetha School of Engineering, Saveetha Institute of Medical and Technical Sciences (SIMATS), Chennai – 602 105, Tamil Nadu, India.

Abstract

Copper Sulfide (CuS) was successfully synthesized using a simple method using two batches of co-solvent (30:70 ratio) with 0.5 M of sodium hydroxide and 0.2 M of Copper acetate at pH~12. 30% ethanol and 70% deionized water (DW) make up the co-solvent sample in batch one; in batch two, 30% ethylene glycol is used as instead; these samples are referred to as Et30:70 and EG30:70, respectively. Spectrophotometers are used to analyse the optical characteristics, size, shape, and structure. Samples Et30:70 and EG30:70 are exhibiting band gap at 2.23 eV and 1.22 eV, respectively. The outcome demonstrates that the visible and near-infrared areas are where the absorption wavelength is located. Et30:70 was found to have somewhat higher calculated optical characteristics than EG30:70, with the exception of extinction efficiency.

Keywords: Hexagonal Covellite, Co-solvents, stoichiometric, X-Ray diffraction, Optical properties.

Manuscript

1. Introduction

Copper sulfide is an economical transition metal chalcogenide, well known for its Ptype semiconducting property with 1.2 - 2.35 eV band gap (falling in visible region) due to 3doribital electron effect. Allowing privileging in building photo-electro-chemical and biooptical devices because of its tuneable energy band gap, enhancing charge carrier activity and producing excellent electronic, thermal and magnetic properties. Compounds of copper sulfides can be categorized into stoichiometric and non-stoichiometric forms, contingent upon the Cu: S compositional ratio, which may indicate a copper-rich or sulfur-poor configuration, and vice versa [1]. Major Copper sulfide phases includes Covellite (Cu(II)S or CuS), Chalcocite (Cu(I)S or Cu₂S) [2], Villamaninite (CuS₂), Djurleite (Cu_{1.95}S/ Cu₃₁S₁₆/ Cu₆₂S₃₁), Anilite (Cu_{1.75}S/ Cu₇S₄), Digenite (Cu_{1.8}S / Cu₉S₅) [3, 4], Greerite (Cu_{1.6}S), Spinonkopite (Cu_{1.39}S), Yarrowite (Cu_{1.12}S) [5] all of them manifest a metallic and brittle nature, displaying a diverse array of appearances and properties, thereby rendering them suitable for various applications. The attainment of alloys of copper sulfides shows considerable challenges; however chemical synthesising of them as compounds or composites can be readily achieved at ambient temperature and under atmospheric conditions. Copper 'Cu' ore represents a transition metal that is typically basic in its characteristics, whereas sulfur 'S' ore belongs to the non-metallic chalcogenide category, exhibiting acidic properties, which accounts for its distinctive rotten egg odour. Both the ores are commercially sustainable and poses diamagnetic properties. The fundamental physicochemical characteristics of this ore are presented in Table. 1. While 'S' chalcogenide has a flammability risk with O₂, 'Cu' metal forms a green coating when exposed to moisture and CO₂ in the air. However, composites of Cu and S have no such risks, so their disadvantages are balanced. They become non-flammable and non-toxic, and they have improved photothermal and electro-optical conductivity with low electronegativity.

Because of these characteristics, researchers have recently focused on creating Copper sulfides as binary, ternary, and quaternary [6] at the nanoscale (1D and 2D) as nanowires [7], nanosheets, or as quantum dots (0D), thin films [8], with heterostructures [9, 10], by adjusting its energy band and using it for a variety of purposes based on the objectives. They are extensively studied in energy harvesting devices (microbial fuel cells [11], photovoltaic cells (pervoskite, DSSC [12], QDSSC); as electrodes (counter electrodes, transparent conducting electrodes); as energy storage devices (supercapacitors, rechargeable batteries [13]; as memory chips/devices [14]; as sensors (IR sensors [15], glucose/bio sensors [40]; as sewage/wastewater treatment (WWT); as electrocatalysis or photocatalytic water splitting and many more built by various physicochemical synthesizing techniques. Hydrothermal, solventless thermolysis, magnetron sputtering, co-precipitation, and chemical bath deposition are some of the recent techniques employed to build their phases. Among them Co-precipitation is the most straightforward, cost-effective, and efficient method for creating nanoparticles (NPs) in ambient settings. Copper-based reagents such as CuC₁₂, Cu (CH₃COO) 2, and CuSO₄ are frequently utilized, whereas sulfur-based reagents include Na₂S, SC (NH₂)₂, and Na₂S₂O₃ [16]. The band gap and absorption behaviour of NPs are influenced by their nanosize, and high surface energy which allows for high mobility in electrochemical and biochemical effectively inorganic reactions, it removes both organic and pollutants/contaminants, leading to high catalytic efficiency.

The CuS phase of copper sulfide powder particles is generated at the nanoscale using two distinct organic co-solvents in the study that is being presented. Their structure, morphology, presence of functional groups, and optical characteristics are reported that were analysed using several spectrometers.

2. Experimental

2.1. Materials

Cupric (II) acetate monohydrate (99%, Merck), sodium sulfide hydrate (60%, LobaChemie), ethanol (99.9%, merck), ethylene glycol, acetone (99%, Qualikems). All the reagents are of analytical grade used without further purification.

2.2. Preparation of CuS nanoparticles

In two batches, 0.2 M copper acetate is dissolved; 30:70 ml of ethanol: DW is in beaker one, and 30:70 ml of ethylene glycol: DW is in beaker two. The copper reagent was spontaneously dissolved by these organic solvents, giving the solution a blue tint. After three hours of continuous magnetic stirring with 0.5 M sodium sulfide dissolved in 50 ml DW, it turned black, causing black precipitates of copper sulfides. Using distilled water and acetone, the precipitates are centrifuged three times before being filtered and dried for half an hour on a hot plate. For characterisation, it was post-annealed for two hours at 200 °C in a muffle furnace and then ground using a mortar and pester (Fig. 1(a)).

2.3. Growth mechanism

I. Dissolution of Copper (II) acetate

$$Cu(CH_3 COO)_{2(s)} \xrightarrow{H_2O} Cu^{2+}_{(aq)} + 2 CH_3COO^{-}_{(aq)}$$
 (1)

II. Dissolution of Sodium Sulfide in water

$$Na_2 S_{(s)} \xrightarrow{H_2 O} S^{2-}_{(aq)} + 2 Na^+_{(aq)}$$
 (2)

The pH is unaffected by Na⁺ ions. Hydrosulfide (HS⁻) (pH \sim 8–12) and hydrogen sulfide (H₂S) (pH \sim 4–7) are the two hydrolysis products of the strong base S²⁻ (pH > 12), which reacts with water instantly. However, there is enough free S⁻ to react with Cu⁺ ions (metal ions) in basic conditions or when there is enough sulfide.

III. Precipitation of CuS

$$Cu^{2+}_{(aq)} + S^{2-}_{(aq)} \to CuS_{(s)} \downarrow$$
 (3)

2.4. Characterization

The Analytical X'Pert PRO powder "X-ray Diffractometer," which operates at 40 kV and 30 mA and uses a CuK α radiation (λ = 1.5425 Å) source. The DLaTGS-detector-equipped Thermo Nicolet 380 "FTIR Spectrophotometer" measures wavelengths between 4000 and 400 cm⁻¹ with an accuracy of 0.01 cm⁻¹ and a resolution of 0.5 cm⁻¹. Morphology and composition analyses was done with "Scanning Electron Microscopy" and "Energy Dispersive X-Ray" at an operating voltage of 20 kV. Thermofisher Evaluation 220's "UV Diffuse Reflectance Spectroscopy" was used to identify the absorption peaks at wavelengths between 190 and 1100 nm.

3. Results and Discussion

3.1. Structure

The prepared samples closely matched the hexagonal (CuS) covellite phase standard (JCPDS: 06-0464). At 12°, 18°, 27°, 29°, 31°, 44°, 47°, 52°, and 59°, its 20 (°) peaks appeared, all of which are consistent with earlier findings (Figure 2). By confirming its hexagonal structure with " $a = b \neq c$ " and " $\alpha = \beta \neq \gamma$," the peak intensity at 47.92° (1 1 0) typically matches to the hexagonal plane, confirming its structure. There were no more contaminants found. 16.4% and 16.6% crystallinity were obtained using batch 1 and batch 2 co-solvents, respectively. Using the Debye-Scherer formula Eq.4, the average crystallite size (D) of the samples was found to be at the nano level. The lattice constant of the produced samples was estimated using the (h k l) values from Eq.5, and it matched the literature well.

$$\left[D = \frac{0.9 \times \lambda}{\beta \times \cos\theta}\right] \tag{4}$$

$$Hexagonal: \frac{1}{d^2} = \frac{4}{3} \left(\frac{h^2 + k^2 + hk}{a^2} \right) + \frac{l^2}{c^2}$$
 (5)

Sample Et_{30:70} has a significant dislocation density and microstrain (Table. 2). In comparison to the EG_{30:70} sample, it reveals that the Et_{30:70} sample has greater imperfections in its surface and crystal dislocation. During the degradation process, this crystal flaw will offer active sites for dye adsorption. The constructed Et_{30:70} sample has the potential to function as an effective photocatalyst; in fact, its band gap (2.23 eV) supports this claim by permitting adsorption in the visible region, which is essential for dye degradation.

3.2. Morphology

SEM images of samples Et_{30:70} (Fig. 3(a)) and EG_{30:70} (Fig. 3(b)) at 200 nm magnification reveal densely packed clusters of irregular partials. Their SEM also shows surface roughness with agglomeration. Sample with Ethylene glycol co-solvent (EG_{30:70}) seems slightly larger in partial size in comparison to Et_{30:70} conforming with calculate 'D' value from Scherrer equation.

3.3. FTIR

The blue curve in Fig. 4 for Sample Et_{30:70} shows that the N-H is responsible for the peak at 3468 cm⁻¹, the O-H group is responsible for the peak at 2976 cm⁻¹, the CH₂ symmetric stretch is at 2884 cm⁻¹, the C=O aromatic stretch is at 1461 cm⁻¹, the C-N/C-C stretching is at 1046 cm⁻¹, the NH₂ wagging is at 839 cm⁻¹, and the C-H aromatic bending is at 586 cm⁻¹. For EG_{30:70} (red curve), the O-H (alcohol) peak is at 3452 cm⁻¹, the O-H (acidic) peak is at 3129 cm⁻¹, the nitro compound N=O symmetric peak is at 1337 cm⁻¹, the C-O single bond is at 1032 cm⁻¹, the N-H wagging is at 725 cm⁻¹, and the C-H bending is at 579 cm⁻¹.

3.4. UV Diffuse Reflectance Spectroscopy

The first absorption shift for $Et_{30:70}$ occurred at 439 nm, which is in the visible (bluish-violet) area, while a minor absorption shift for $EG_{30:70}$ took place at 820 nm, which is in the near infra-red region (Fig. 5(a)). Theoretically, the band gap is determined using Eq. 15, where "v" is the frequency at which sunlight is emitted, "n" is an integer, "Eg" is the band energy in

electron volts (eV), "A" is an energy-dependent constant, " α " is adsorption efficiency, and the Planck's constant "h," which has a value of 6.62607015 x 10^{-34} (joule second or m_2 kg/s). For the Et_{30:70} (Fig. 5(b)) and Et_{30:70} (Fig. 5(c)) samples, the energy band gap between valance and conduction was 2.23 eV and 1.22 eV, respectively.

$$\alpha h \nu = A \big(h \nu - E_g \big)^n \tag{6}$$

The transmittance percentage (Ts), where Io is the light intensity transmitted, is always a logarithmic function of absorbance (A) (Eq. 7). This 'Ts' value is essential in calculating refractive index (n) (Eq. 8) of the materials because it is the measure of light propagating through a material. Thus 'n' value plays an importance in optical devices designing. If 'n' is high, light passes more slowly through a substance because its direction changes. Other optical parameters such as extinction coefficient, real and imaginary part of dielectric constants, optical conductivity and dielectric susaptibility are theoretical deriver for adsorption edge and listed in Table.3.

$$A = \log 10 \left[\frac{1}{T} \right] = \log 10 \left[\frac{I_0}{I} \right] \tag{7}$$

$$n = \frac{1}{T_S} + \sqrt{\frac{1}{(T_S - 1)}} \tag{8}$$

4. Conclusions

Two distinct chemical co-solvents (30:70 ml ratio) are used to successfully synthesis the hexagonal (CuS) covellite phase at room temperature. The samples' band gaps were 2.23 eV and 1.22 eV, respectively, while their average crystallite sizes at the nanoscale were 5.34 and 6.71 nm. At an arrangement of 2.3 E^7 , both samples had its optical conductivity. Every spectrometer parameter that is produced is calculated theoretically and displayed in the appropriate tables and diagrams. It demonstrates that the sample's microstrain was high when ethanol was used as a co-solvent ($Et_{30:70}$). The $Et_{30:70}$ sample had somewhat greater average crystallite size, dislocation density, and optical characteristics such as band gap, refractive

index, real and imaginary dielectric constant, and dielectric susceptibility than the EG_{30:70} sample.

CRediT to Author contributions

Shanthosh Shree S: Writing – Original draft, Conceptualization, Data curation, Formal analysis, Investigation, Methodology, Visualization.

Dr. S Thanikaikarasan: Writing – Review and editing, Supervision, Investigation; Resources, Validation, Conceptualization.

Declaration of Competing Interest

The authors declare that they have no Known competing financial interests or personal relationships that could have appeared to influence the reported work in this paper.

Data Availability

The data that has been used is confidential.

Acknowledgements

The authors of this study thankfully acknowledge the support provided by Saveetha School of Engineering, Saveetha Institute of Medical and Technical Sciences for provide the opportunity to carry out the research work

Conflict of Interest Statement

There are no conflicts of interest to declare regarding this paper. Moreover, the project entails no involvement in human or animal testing, along with any usage of dangerous or hazardous substances and equipment. Therefore, the current investigation is expected to produce no relevant ethical issues.

5. References

- [1] Sharma, L. K., Kar, M., Choubey, R. K., & Mukherjee, S. (2021). Low field magnetic interactions in the transition metals doped CuS quantum dots. *Chemical Physics Letters*, 780, 138902.
- [2] Agarwal, S., Phukan, P., Sarma, D., & Deori, K. (2021). Versatile precursor-dependent copper sulfide nanoparticles as a multifunctional catalyst for the photocatalytic removal of water pollutants and the synthesis of aromatic aldehydes and NH-triazoles. *Nanoscale Advances*, 3(13), 3954-3966.
- [3] Xue, J., Ren, D., Wang, S., Bu, X., Song, Z., Zhao, C., & Chen, T. (2021). Effect of ferric ions on sulfidization flotation of oxidize digenite fine particles and their significance. *Minerals*, 11(3), 305.
- [4] Xue, J., Ren, D., Chen, T., Bu, X., Wan, H., Song, Z., & Zhao, C. (2021). Hydrophobic agglomeration flotation of oxidized digenite fine particles induced by Na2S and butyl xanthate. *Minerals Engineering*, 168, 106932.
- [5] Ravele, M. P. (2022). Copper chalcogenide nanoparticles as photocatalysts for the removal of pharmaceuticals from water (Doctoral dissertation, North-West University (South Africa)).
- [6] Li, Y., Liu, Z., Chen, J., Wang, S., Lin, O., Yang, C., & Tang, A. (2024). Recent advances in quaternary copper-based sulfides and their derivatives for solar hydrogen evolution. *Journal of Materials Chemistry A*.
- [7] Anichini, C., Czepa, W., Aliprandi, A., Consolaro, V. G., Ersen, O., Ciesielski, A., & Samorì, P. (2021). Synthesis and characterization of ultralong copper sulfide nanowires and their electrical properties. *Journal of Materials Chemistry C*, 9(36), 12133-12140.
- [8] Mohammed, K. A., Ahmed, S. M., & Mohammed, R. Y. (2020). Investigation of structure, optical, and electrical properties of CuS thin films by CBD technique. *Crystals*, 10(8), 684.
- [9] Mishra, D., Kim, S., Kumar, N., Krishnaiah, M., & Jin, S. H. (2023). Self-discharge mitigated supercapacitors via hybrid CuO-nickel sulfide heterostructure for energy efficient, wireless data storage application. *Journal of Materials Science & Technology*, 147, 77-90.

- [10] Marimuthu, T., Yuvakkumar, R., Ravi, G., Zheng, Y., Bi, Z., Xu, X., & Velauthapillai, D. (2022). One-step fabrication of copper sulfide catalysts for HER in natural seawater and their bifunctional properties in freshwater splitting. *Fuel*, *322*, 124073.
- [11] Wu, Shanshan, et al. "Copper removal and elemental sulfur recovery from fracturing flowback water in a microbial fuel cell with an extra electrochemical anode." Chemosphere 303 (2022): 135128.
- [12] Kaur, K., Patyal, M., & Gupta, N. (2021). A review on the use of carbon matrix incorporated with macrocyclic metal complexes as counter electrodes for platinum free dye sensitized solar cells. *Journal of Coordination Chemistry*, 74(4-6), 543-562.
- [13] Kalimuldina, G., Nurpeissova, A., Adylkhanova, A., Adair, D., Taniguchi, I., & Bakenov, Z. (2020). Morphology and dimension variations of copper sulfide for high-performance electrode in rechargeable batteries: a review. *ACS Applied Energy Materials*, 3(12), 11480-11499.
- [14] Fei, Y., Man, Y., Sun, J., Du, Y., Chen, B., Bao, J., & Zhou, X. (2023). Implanting CuS Quantum Dots into Carbon Nanorods for Efficient Magnesium-Ion Batteries. Small, 19(34), 2301954.
- [15] Mohamed, S. H., Awad, M. A., Hafez, M. I., & Hadia, N. M. A. (2021). Change in properties upon thermal treatment of copper sulphide powder and thin films. *Bulletin of Materials Science*, 44, 1-11.
- [16] Jiang, X., Xie, Y., Lu, J., He, W., Zhu, L., & Qian, Y. (2000). Preparation and phase transformation of nanocrystalline copper sulfides (Cu₉S₈, Cu₇S₄ and CuS) at low temperature. Journal of Materials Chemistry, 10(9), 2193-2196.

Figure caption(s)

Figure 1 (a) CuS nanoparticle preparation; (b) CuS phase unit cell structure construction.

Figure 2 XRD of synthesised CuS samples: Et_{30:70} and EG_{30:70}.

Figure 3 SEM image of (a) Et_{30:70} and (b) EG_{30:70} samples.

Figure 4 Fourier Transform Infrared Spectrum.

Figure 5 (a) UV-DRS adsorption curve, and (b) tauc's plot (direct band gap).

Table caption(s)

Table 1 Stoichiometric covellite phases' general structural characteristics (CuS).

Table 2 Theoretical derived XRD parameters for built samples Et_{30:70} and EG_{30:70}.

Table 3 Optically determined parameters for CuS samples prepared with different cosolvents.

Figure 1

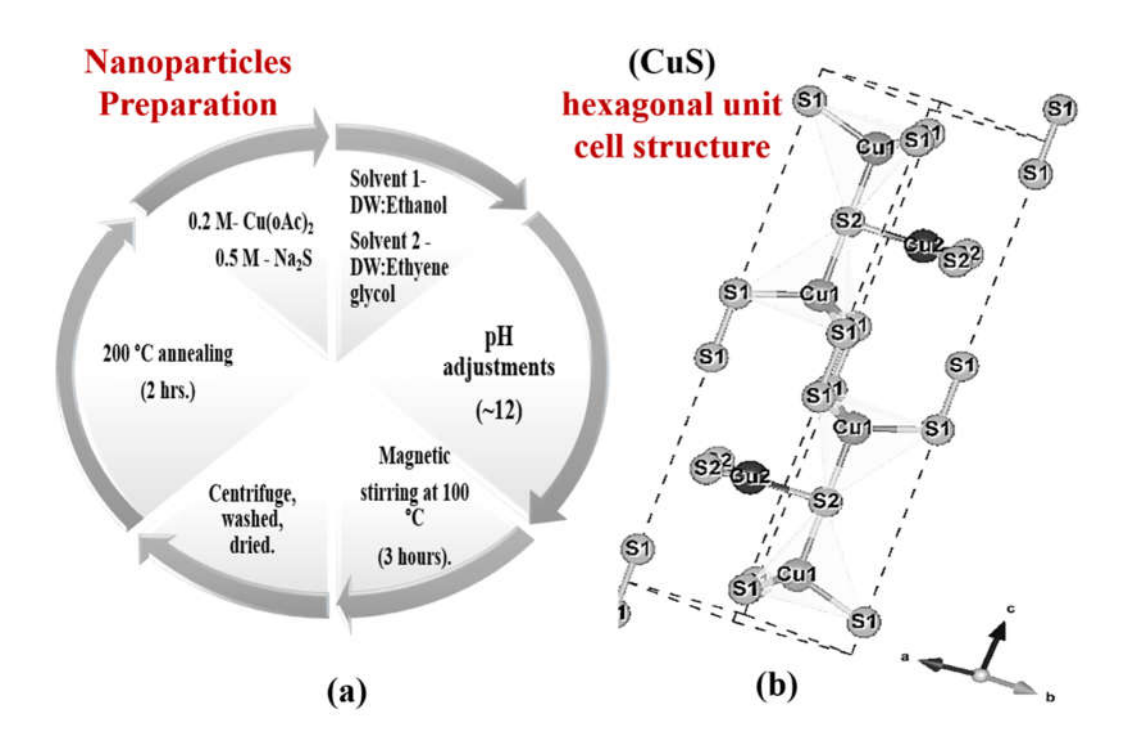


Figure 2

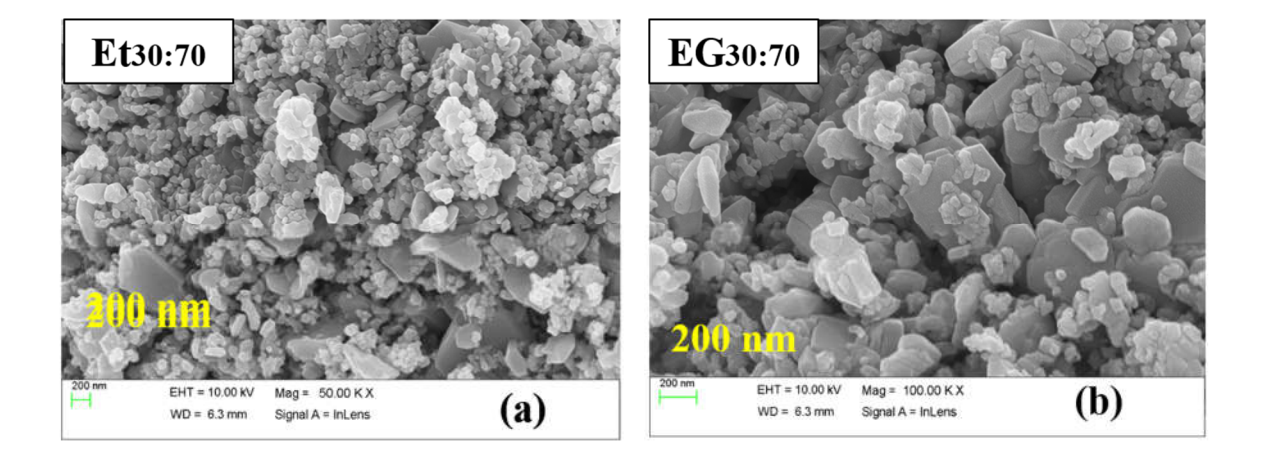


Figure 3

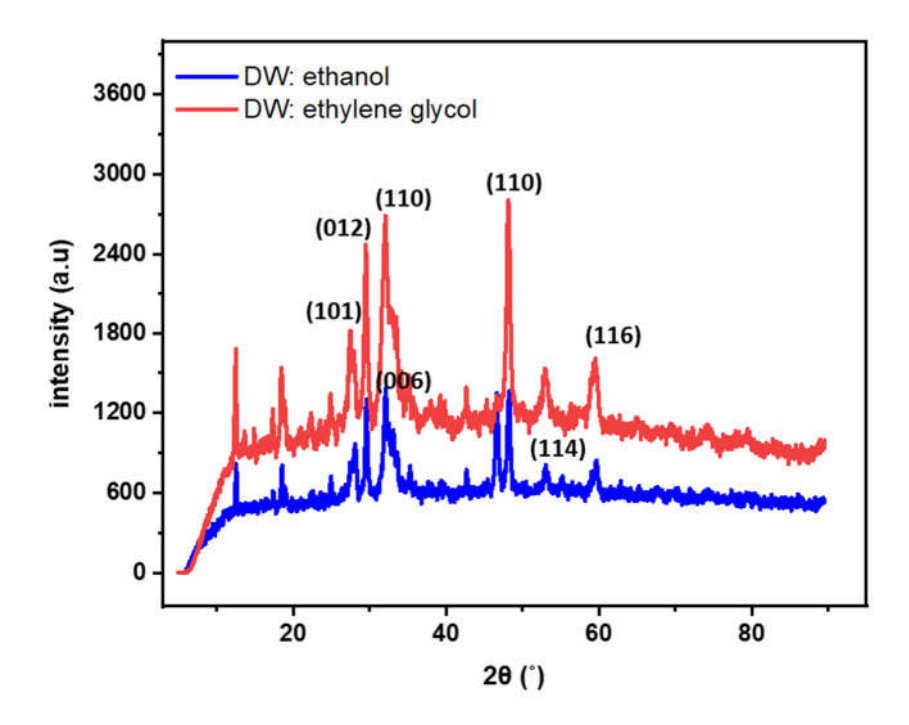


Figure 4

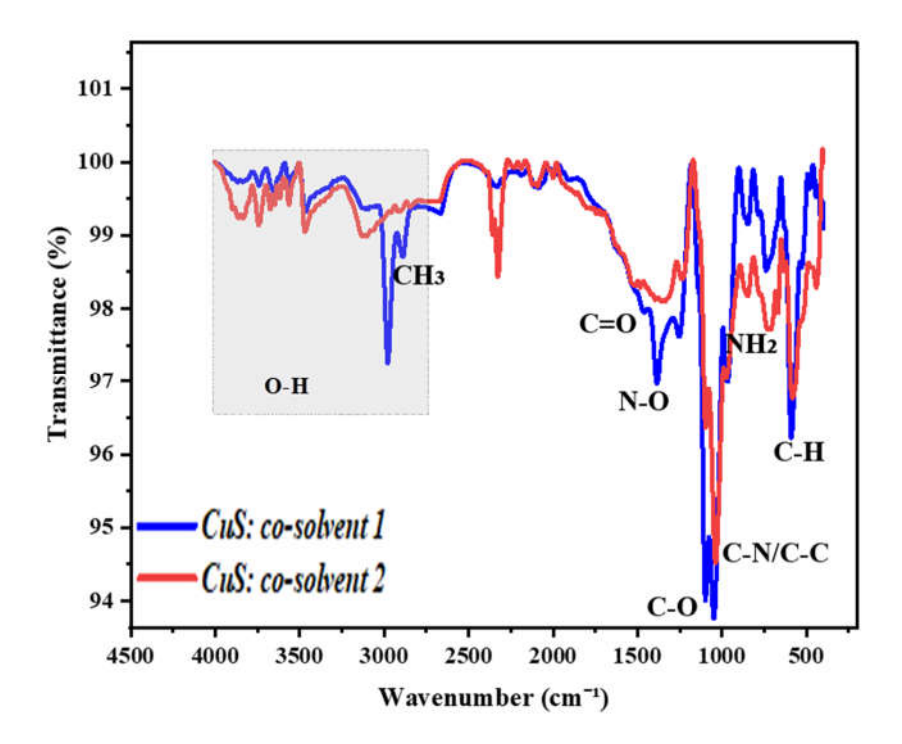


Figure 5

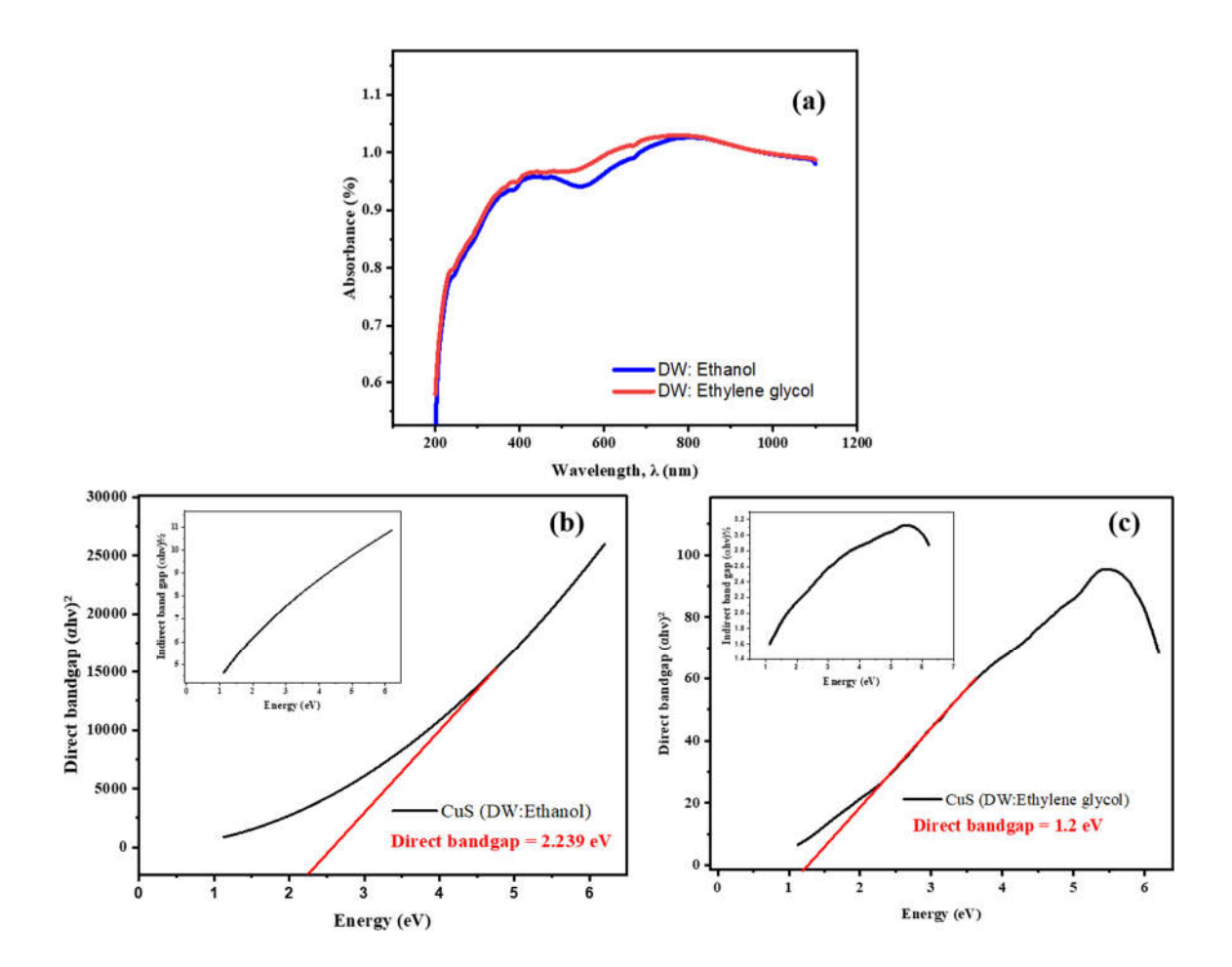


Table 1

Phase name	Covellite							
Chemical Formula	CuS (Stoichiometric)							
Crystal System	Hexagonal							
Colour	Indigo -blue or darker, Brass -yellow to deep red.							
Tenacity	Flexible							
Thermal stability	180 °C							
Space Group	P63/mmc							
Lustre	Submetallic							
Lattice constants	$a = b \neq c,$ $\alpha = \beta \neq \gamma$							
Unit Cell Parameter	a = 3.7938 Å; c = 16.341 Å; $Z = 6$. $Z = 6$.							

Table 2

CuS Co- solvent	Crystal structure	Co - solvent (30:70 ratio)	Mapped 2θ(°)	Lattice constant (a = b ≠ c)	(h k l) planes	d- spacing (nm)	Average crystal Size, D (nm)	Microstrain $\left[\varepsilon = \frac{\beta}{4\tan\theta}\right]$	Dislocation density $\left[\delta = \frac{1}{D^2}\right]$
Et30:70	Hexagonal	Ethanol: DW	32.19	a=3.8 A°; c=16.3 A°	006	2.75	5.34	283.2467	0.035069
EG30:70	Hexagonal	Ethylene Glycol: DW	47.92	a=3.7 A°; c=16.3 A°	110	0.18	6.71	-48.4734	0.02221

Table 3

CuS	Wavele	Absorpti	Dire	Refracti	Extincti	Real	Imagina	Optical	Dielectric
samples	\textbf{ngth},λ	on	ct	ve index	on	dielect	ry	Conductiv	susceptibility
name	(nm)	region	Ban	(n)	coefficie	ric	dielectri	ity	$\chi = [\varepsilon_1] - 1 -$
			d		nt [k =	consta	c	σ	L
			gap		$\frac{\alpha\lambda}{4\pi}$	nt	constant	$=\frac{\alpha nc}{4\pi}$	$\left[\frac{1}{4\pi}\right]$
			(eV)		4π]	$[\epsilon_1=n^2-$	$[\epsilon_2=2nk]$	4π]	
						k^2]			
Et30:70	436	Visible	2.23	0.0023	178.4	-3183	0.820	$2.395 E^7$	-3183
EG30:70	820	NIR	1.22	0.0012	335.5	-1126	0.818	2.389 E ⁷	-1126